Geophysical Research Letters®

Key Points:

- A survey of 22 Alpine glaciers shows increased margin collapse frequency linked to rapid climate warming since the 1980s
- Collapse appears to be associated with glacier thinning, stagnation of snout margins and reduced rates of subglacial channel closure
- Intensive study of a collapse event confirms that up-glacier extension of an unpressurized subglacial channel drives the collapse process

Author Contributions:

Conceptualization: Pascal E. Egli, Stuart N. Lane
Data curation: Pascal E. Egli
Formal analysis: Pascal E. Egli, Bruno Belotti, Stuart N. Lane
Funding acquisition: Stuart N. Lane
Investigation: Pascal E. Egli, Bruno Belotti, Boris Ouvry, Stuart N. Lane
Methodology: Pascal E. Egli, Bruno Belotti, Boris Ouvry, Stuart N. Lane
Project Administration: Stuart N. Lane
Resources: Pascal E. Egli

Subglacial Channels, Climate Warming, and Increasing Frequency of Alpine Glacier Snout Collapse

Pascal E. Egli[1] , **Bruno Belotti[2]** , **Boris Ouvry[3], James Irving[4]** , and **Stuart N. Lane[1]**

[1]University of Lausanne, Institute of Earth Surface Dynamics, Lausanne, Switzerland, [2]Department of Geological Sciences, University of Idaho, Moscow, ID, USA, [3]University of Zurich, Institute of Geography, Zurich, Switzerland, [4]University of Lausanne, Institute of Earth Sciences, Lausanne, Switzerland

Abstract Alpine glacier retreat has increased markedly since the late 1980s and is commonly linked to the effects of rising temperature on the surface melt. Less considered are processes associated with glacier snout-marginal surface collapse. A survey of 22 retreating Swiss glaciers suggests that collapse events have increased in frequency since the early 2000s, driven by ice thinning and reductions in glacier-longitudinal ice flux. Detailed measurement of a collapse event at one glacier showed 0.02 m/day vertical surface deformation above a meandering main subglacial channel. However, with low rates of longitudinal flux (<1.3 m/year), this was insufficient to close the channel in the snout marginal zone. We hypothesize that an open channel maintains contact between subglacial ice and the atmosphere, allowing greater incursion of warm air up-glacier, thus enhancing melt from below. The associated meandering of subglacial channels at glacier snouts leads to surface collapse and removal of ice via fluvial processes.

Plain Language Summary Mountain glaciers have been melting and retreating more rapidly since the onset of accelerated atmospheric warming in the late 1980s. Our study examines 22 Swiss glaciers in order to understand why, for some glaciers, the ice surface close to the glacier margin breaks down and forms collapse features, and for others, it does not. We find that the combination of thin ice having a low surface slope results in locally reduced ice flow, which causes subglacial channels to close more slowly and eventually leads to channel roof collapse. A detailed study based on ground-penetrating radar and drone surveys at one of the glaciers showed that the subglacial channel there is very wide and shallow, and that its strongly sinuous shape may have contributed to a recent ice-surface collapse. Ice blocks from the melting and collapsing channel were flushed out by the proglacial stream. We observe that such collapse features have become more frequent as air temperatures increase. Visibly, they may contribute to more rapid glacier recession.

1. Introduction

Alpine glaciers have been retreating rapidly since the 1980s because of rapid climate warming (Diolaiuti et al., 2011; Fischer et al., 2015; Haeberli et al., 2007; Paul et al., 2004; Sommer et al., 2020). The retreat is forecast to accelerate in the coming decades (Zekollari et al., 2019). The primary mechanism of mass loss for Alpine glaciers is surface melt (Arnold, 2005; Oerlemans & Knap, 1998; Vincent et al., 2004). Negative glacier mass balance can also be driven by reduced snow accumulation. Less considered is basal or internal ablation. This can involve the collapse of subglacial channels in the snout marginal zone, driven by thinning ice combined with slow creep closure. After the collapse, ice is removed via the channel to the glacier outlet. This mechanism of glacier retreat was first described some time ago as "subglacial stoping" or "block caving" (Loewe, 1957; Paige, 1956).

There are very few documented or quantified examples of this process (Bartholomaus et al., 2011; Dewald et al., 2021; Kellerer-Pirklbauer & Kulmer, 2019; Konrad, 1998; Lindström, 1993; Stocker-Waldhuber et al., 2017). As a result, little is known about where and when collapse features form and whether or not their formation frequency is changing due to climate warming. We hypothesize that their formation is driven by three interconnected mechanisms: (a) long-term negative mass balance leads to shallow ice in glacier snout margins, (b) shallow ice means reduced longitudinal ice flow velocities and reduced creep closure of subglacial channels, and (c) presence of a subglacial channel underneath shallow ice can initiate collapse due to upwards melting and detachment of ice blocks.

Software: Pascal E. Egli, Bruno Belotti, James Irving
Supervision: James Irving, Stuart N. Lane
Validation: Pascal E. Egli
Visualization: Pascal E. Egli, Bruno Belotti
Writing – original draft: Pascal E. Egli, Bruno Belotti
Writing – review & editing: Pascal E. Egli, James Irving, Stuart N. Lane

Here, we perform statistical analysis on a sample of 22 Swiss glaciers based on 24 glacier properties, climate data, and historical aerial imagery in order to investigate how pervasive these collapse events are becoming and to test the abovementioned hypotheses. We support our conclusions with the intensive study of a retreating glacier, Glacier d'Otemma, which experienced a recent (2017–2018) collapse event and where we measured ablation, surface elevation change, flow speed, and the position of a principal subglacial channel in the snout zone.

2. Materials and Methods

2.1. Overview

Conditions driving snout margin collapse were examined by analysis of topography, ice thickness, historical aerial imagery, air temperature, and glacier length change data for 22 glaciers in the western and central Swiss Alps (Figure 1). We focus on Swiss glaciers because of the widespread availability of measurements, notably glacier bed topography, ice thickness, and aerial imagery, from which we could build an extensive database of the conditions at glacier snout margins. We focus on a single region under the assumption that all glaciers should have experienced relatively similar climate warming. Based on historical and contemporary aerial imagery, 12 glaciers were selected that showed at least one subglacial channel collapse feature near their terminus since 2015. In addition, 10 glaciers not exhibiting collapse features since 1938 (the first imagery date) were chosen in order to do a balanced statistical comparison (Figure 1). Their choice reflected (a) relatively close proximity to the glaciers where collapse was observed, (b) having comparable topography and size to nearby glaciers with collapse features, and (c) being in the databases we used to calculate glacier retreat, topography, and ice thickness.

Second, we examined in detail the ice surface lowering, subglacial channel position, and ice ablation measured using uncrewed aerial vehicle (UAV) imagery, ground-penetrating radar (GPR) measurements, and ablation stakes, respectively, before and during a collapse event at the Glacier d'Otemma (2017–2018). This allowed investigation of the mechanisms leading to collapse and the exent to which unpressurized subglacial marginal channels can extend up-glacier.

2.2. Frequency of Collapse Events

To test whether the frequency of snout marginal channel collapse events is increasing with time, we used the SwissTopo LUBIS visualization system. LUBIS contains all of the digitized aerial imagery held by SwissTopo back to 1938. We inspected the imagery available for each glacier in order to determine whether or not a collapse feature was present. In all cases, collapse features were only observed in snout marginal zones. Each instance showing the snout of one of the glaciers was considered an observation. On some aerial images, several of the chosen glacier snouts were visible, meaning that the same image could be counted more than once. There were 179 observations in total. Of these, 29 showed a collapse feature and 150 did not. To avoid the same collapse feature being counted twice, a collapse observation was only retained if it had the same snout showing no collapse in the last previous observation. On this basis, we removed two counts. We considered the cumulative number of identified collapses through time as compared with the cumulative number of observations made in order to account for an increase in the frequency of image acquisition after 1980.

2.3. Characterization of Collapse Conditions

For each of the 22 glaciers considered, we assembled a database consisting of (a) surface elevation information from the SwissAlti3D Digital Elevation Model (SwissTopo, 2021), (b) bed topography, and ice thickness distribution based on GPR data and modeling (Grab et al., 2021), and (c) length change history information from Glacier Monitoring Switzerland (GLAMOS, 1881–2020). Section S3.1 in Supporting Information S1 explains how this database was compiled. Table S2 in Supporting Information S1 lists the 24 properties considered in our analysis and how they were derived directly (e.g., ice thickness in the snout marginal zone) or inferred from basic process laws. Notably, mean snout marginal glacier velocity was computed as a function of shear stress and ice thickness, using Glen's flow law (Cuffey & Paterson, 2010; Gantayat
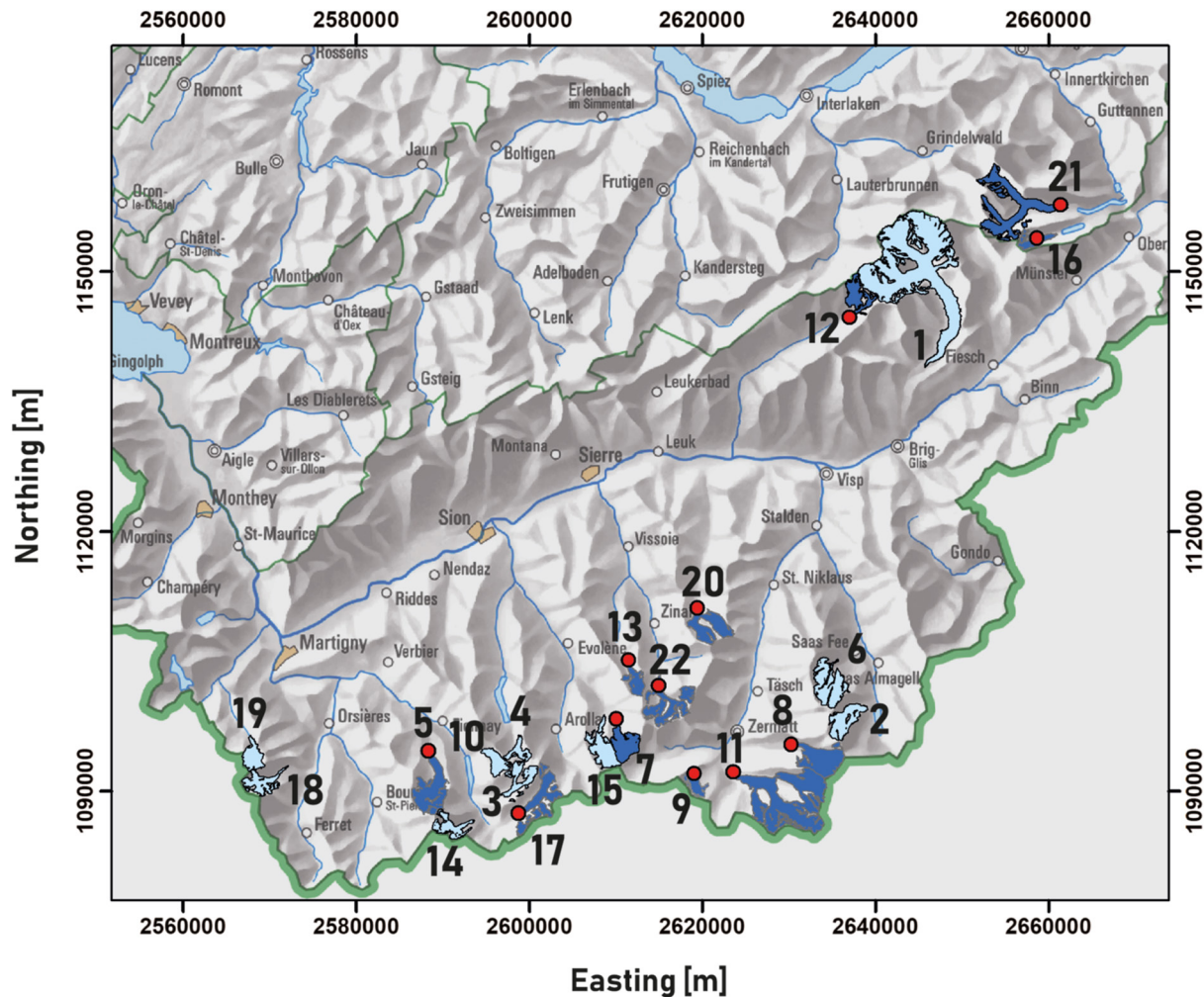
Figure 1. Map showing the 22 glaciers examined in this study. Glaciers in dark blue exhibited a subglacial channel collapse feature in aerial imagery (red points) whereas glaciers in light blue have not had any collapse features since 1938. Coordinates are in the local Swiss Grid CH1903+ system, in meters. Legend: (1) Aletschgletscher,(2) Allalingletscher, (3) Glacier du Brenay, (4) Glacier de Cheilon, (5) Glacier de Corbassière, (6) Feegletscher, (7) Glacier de Ferpècle, (8) Findelgletscher, (9) Furgggletscher, (10) Glacier de Giétro, (11) Gornergletscher, (12) Langgletscher, (13) Glacier de Moiry, (14) Glacier du Mont Durand, (15) Glacier du Mont Miné, (16) Oberaargletscher, (17) Glacier d'Otemma, (18) Glacier de Saleina, (19) Glacier du Trient, (20) Turtmanngletscher, (21) Unteraargletscher, (22) Glacier de Zinal.

et al., 2014; Haeberli & Hölzle, 1995; Section S3.1 in Supporting Information S1), with values comparable to those obtained from large-scale observations (Millan et al., 2019).

To investigate the extent to which glaciers showing collapse features are likely to have lower longitudinal ice flux and subglacial channel closure, we considered mean ice thickness, bed slope, and surface slope for the entire glacier and for the first 2 km of each glacier tongue. These properties were also determined for a 100 m radius around each of the most recent collapse zone locations. As all glaciers showing collapse features had a collapse event between 2015 and 2020, the values of these properties derived for ice thickness distributions dating from 2016 are comparable (Table S6 in Supporting Information S1). The mean distance between the center of the most recent collapse feature and the glacier terminus for the 12 glaciers showing collapse features was found to be ~250 m. Thus, for glaciers not showing collapse features, a hypothetical collapse zone of 100 m radius, positioned at the centerline at a horizontal distance of 250 m from the terminus, was used (details in Section S3.5.1 in Supporting Information S1).

We also characterized glacier length change using Glacier Monitoring Switzerland (GLAMOS, 1881–2020) data to determine length change and variability in length change since 1987, which is the date considered for the onset of rapid recession related to climate warming in the study region (Costa et al., 2018).

Finally, Jarque and Bera (1980) tests of the 22 samples of each property in Table S2 in Supporting Information S1 suggested that 13 out of 24 properties were non-Gaussian. H_0, the null hypothesis, was that the distribution was normal; the test required a probability, *p*, of 0.05 or less, for 95% or more confidence that it can be rejected. Consequently, we used Mann and Whitney (1947) U tests to evaluate whether the 24 properties differed between those glaciers showing channel collapse and those not showing collapse.

2.4. Relationship Between Summer Air Temperatures and Retreat

If collapse formation is driven by incursion of warm air underneath snout margins via unpressurized subglacial channels, we might expect variation in annual snout recession to be more sensitive to mean annual summer air temperature variations than for glaciers where snout recession is driven by temperature effects on surface melt and long-term mass balance. To investigate this hypothesis, we identified for each glacier the year of onset of continuous retreat, using the GLAMOS (1881–2020) database (Section S3.7 in Supporting Information S1). We calculated a time-series of annual retreat rate (R_A, variables are listed in Table S1 in Supporting Information S1) and its mean (R_M) for each glacier for the period of continuous retreat. For the same period, we determined annual mean summer air temperature in the snout region (T_{SA}) and its mean (T_{SM}). This used spatially interpolated and gridded MeteoSwiss data (temperature 2 m above the ground between June 1 and August 31) from the center of the 1×1 km grid cell located closest to the glacier terminus. We determined the coefficient of variation of retreat (R_{CV}) by dividing the standard deviation of retreat by the mean annual retreat rate. We computed the Pearson correlation coefficient between T_{SA} and R_A (P_{RT}) and we calculated the sensitivity of R_A to T_{SA} (S_{RT}) using simple linear regression. Testing for normality using the Jarque and Bera (1980) test allowed us to compare glaciers with and without collapse features using Student's t, for all parameters except S_{RT}. The latter was not normally distributed and so we used the Mann and Whitney (1947) U test.

2.5. Surface Dynamics and Subglacial Channel Collapse at the Glacier d'Otemma

In August 2017, densely-spaced GPR lines were acquired in the snout zone of the Glacier d'Otemma. This region collapsed during the summer of 2018. These lines allowed mapping of the planform of a major subglacial channel (Egli et al., 2021). During the summer 2018 collapse, high-resolution UAV surveys were acquired on August 7 and on August 23. The positions of 54 Ground Control Points were measured on the same days using a differential global positioning system (dGPS) for the purpose of structure from motion multi-view stereo photogrammetry (Section S3.3, Figures S3, S4 and S5 in Supporting Information S1). Ablation measurements were carried out at 49 regularly distributed ablation stakes (Figure S3 in Supporting Information S1).

Digital elevation models (DEMs) were produced applying a standard processing workflow (Gindraux et al., 2017; James et al., 2020; Rossini et al., 2018, Westoby et al., 2012; Section S3.3 and Figure S3 in Supporting Information S1) using Agisoft Metashape© software. A DEM of difference (DoD; dz_{net}) showing the difference in surface elevation between the two surveys (16 days apart) was then computed. Independent validation of the DEM data suggested that the DEM elevations were precise to ±0.011 m such that for 95% confidence of significant change (see Lane et al., 2003), the limit of detection is ±0.031 m. We did not correct the surface elevation change for lateral ice flux as the longitudinal velocity in the snout margin was measured by dGPS at the ablation stakes, as well as from the UAV imagery using the ImGraft template matching algorithm (Messerli & Grinsted, 2015), to be less than 10 cm over 16 days.

To distinguish between ablation and ice dynamics, we consider the measured net surface height change (dz_{net}) to be equal to the sum of components due to vertical deformation ($dz_{dynamics}$) and ablation ($dz_{ablation}$):

$$dz_{net} = dz_{dynamics} + dz_{ablation} \tag{1}$$
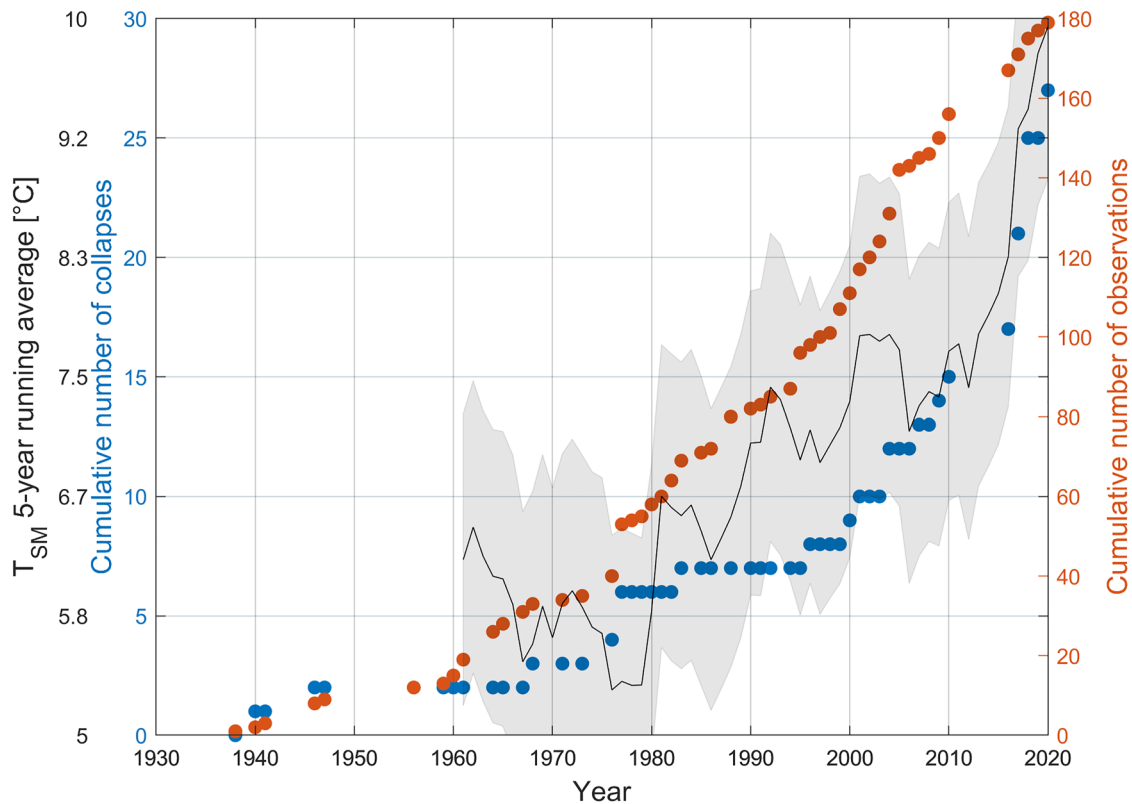
Figure 2. Cumulative number of collapse events (blue dots) and cumulative number of observations (orange dots) since 1938 for all 22 glaciers considered in our study. Five-year running average of the mean summer temperature (T_{SM}, black line) since 1961 over the 12 glaciers exhibiting one or several collapse events, along with the corresponding standard deviation (gray shaded area).

$dz_{ablation}$ was estimated by spatially interpolating ablation stake measurements using kriging. The $dz_{ablation}$ was subtracted from d_{znet} to estimate the surface change due to $dz_{dynamics}$ (Section S3.4 in Supporting Information S1). To test for the influence of variables such as aspect, reflectance, or slope on ice surface elevation changes and melt, we computed their correlations with dz_{net} and $dz_{ablation}$ (Figures S7 and S8; Table S4 in Supporting Information S1). As a proxy for the albedo, we consider surface reflectance (Rippin et al., 2015).

Finally, we tested for a relationship between the presence of a subglacial channel and increased ice surface elevation changes. Based on GPR-derived channel outlines and supported by calculations of the Shreve hydraulic potential (Shreve, 1972; Figure S14 and Section S3.2 in Supporting Information S1), ablation stakes were classified according to the likelihood that they were located over a subglacial channel (Section S3.8 in Supporting Information S1).

3. Results

3.1. Collapse Events and Their Changing Frequency

The most recent channel collapse features identified for the "collapse" glaciers are illustrated in Figure S1 in Supporting Information S1. They differ in the detail of their form, but most have concentric crevasse-like features present in the early stages of development (e.g., Figures S1c and S1i in Supporting Information S1), during collapse (e.g., Figure S1a in Supporting Information S1) and afterward (e.g., Figures S1e and S1j in Supporting Information S1). The images confirm that they can develop in both debris-free and debris-covered snout marginal zones.

Figure 2 shows the cumulative number of collapse events observed on the aerial images, along with the cumulative number of observations from 1938 to the present. The 5-year running average and standard deviation of the mean summer air temperature of "collapse" glaciers are also shown. There is an increase

in the frequency of observations starting in the early 1980s. However, the frequency of observed collapse events increases more rapidly after the year 2000, especially from 2016 to the present. As climate warming accelerates and as glacier retreat continues, so does the collapse frequency.

3.2. Statistical Analysis of Collapse Conditions

Application of the Mann-Whitney U test with a 95% confidence interval to all 24 properties (Table S2 in Supporting Information S1) shows that collapse and non-collapse groups of glaciers only differ significantly for five variables (Figure S2 in Supporting Information S1) within the vicinity of the collapse areas: (a) ice thickness (Figure S2a in Supporting Information S1), (b) creep closure rate (Figure S2b in Supporting Information S1), (c) ice flow velocity (Figure S2c in Supporting Information S1), and (d) mean surface slope (Figures S2d and S2e in Supporting Information S1). Thus, relatively thin ice, a shallow surface slope, and low longitudinal flow velocity near a marginal subglacial channel are the conditions required for collapse. Ice with a thickness of less than 50 m, for example, results in creep closure being small enough that a subglacial channel with a diameter of 5 m does not close over winter (calculations according to Section S3.1, Table S7 in Supporting Information S1). Combined with a small surface slope (a median of 11.4° for glaciers with collapse features; Table S7 in Supporting Information S1) and a small bed slope (a median of 14.3° for glaciers with collapse features; Table S7 in Supporting Information S1) this shallow ice has low glacier-longitudinal flux, further inhibiting channel closure.

3.3. Relationship Between Summer Air Temperatures and Retreat

Mean annual glacier length change, mean summer temperature in the snout zone and the coefficient of variation of retreat did not differ significantly between glaciers exhibiting and not exhibiting collapse features (Student's t, $p = 0.05$). However, glaciers with collapse features had systematically more negative correlations between annual glacier length change and mean annual summer temperature ($p < 0.05$) and higher sensitivity of annual glacier length change to mean annual summer temperature ($p < 0.05$; Figure S11 in Supporting Information S1). For the glaciers with collapse features, 6 out of 12 had significant ($p < 0.05$) negative P_{RT} values compared with two out of 10 non-collapse glaciers. Thus, a diagnostic characteristic of glaciers showing collapse features appears to be a stronger sensitivity to mean summer temperature.

3.4. Measurement of an Active Collapse at the Glacier d'Otemma

Figure 3a shows the UAV-based orthoimage of the Glacier d'Otemma for August 7, 2018, ablation stake positions and location of a more than 10-m-wide subglacial channel based on high-resolution GPR data acquired the year before (Egli et al., 2021). The orthoimage shows the development of a collapse feature close to the glacier snout near the downstream end of the identified channel.

Figure 3b shows the surface elevation changes between August 7 and 23, 2018. General surface height loss is observed all along the glacier tongue. This loss is greatest (up to 1.1 m) in areas of bare ice and reduced where there is greater debris cover (Figures 3a and 3b). Figure 3b also shows increased lowering of the surface above the GPR-identified subglacial channel. Areas outside of the glacier outline show little vertical change, with the exception of zones of 'dead ice' melt under the debris cover (e.g., top left in Figure 3b).

Figure 3c shows surface change after removal of the kriging-interpolated ablation stake measurements. This results in some differences from the original DoD, but the pattern of strong surface lowering in the vicinity of the subglacial channel persists. Small elevation changes outside the area occupied by ablation stakes are within or close to the limit of detection of the DoD. To rule out drivers of surface change other than the presence of a subglacial channel, we examined correlations between surface change and glacier surface slope, reflectance, aspect, and elevation for small patches (0.5×0.5 m) around each ablation stake location. None of these four variables were correlated with elevation change or ablation rate (Table S4, Figures S7 and S8 in Supporting Information S1). Thus, the surface change (Figure 3c) can be attributed to enhanced vertical deformation related to the presence of a subglacial channel that must have been at atmospheric pressure. Evidently, this enhanced deformation was not sufficient for the channel to close and to become pressurized.
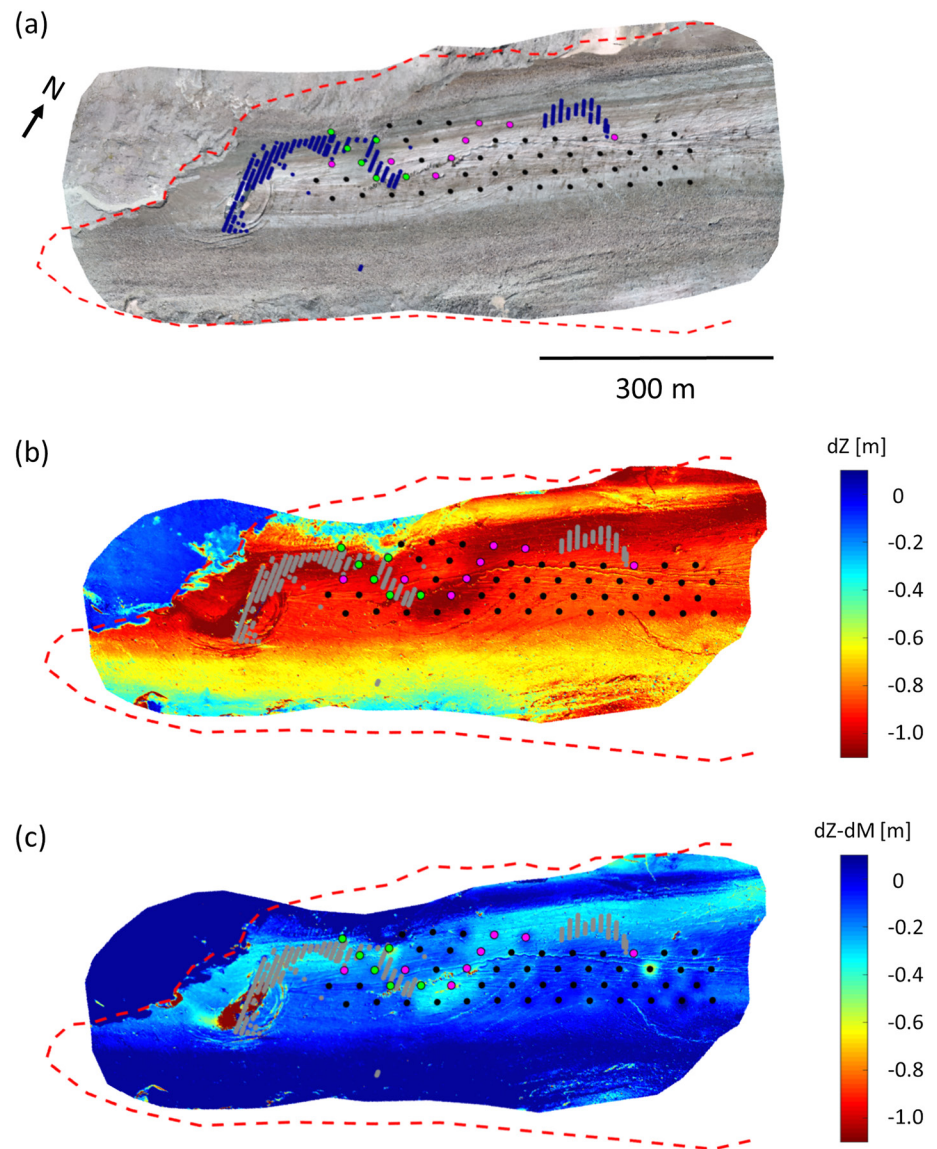
Figure 3. (a) Orthophoto showing the locations of ablation stakes (black dots) and the positions of a major subglacial channel identified using ground-penetrating radar (Egli et al., 2021; blue stipples). (b) Change in surface elevation computed between August 7 and 23, 2018, with channel positions shown as gray stipples. The collapsed area is clearly visible as an elongated dark red spot less than 100 m from the glacier terminus. For readability, the digital elevation model of difference value was clipped to 1.1 m. (c) Image in panel (b) after subtraction of ablation measurements. The ablation stakes are subdivided into off-channel locations (black), almost certainly on-channel locations (cyan), and likely-on-channel locations (magenta).

Surface elevation changes and ablation measurements were compared for three different categories defined according to position: locations known to be above the identified subglacial channel (called on-channel), locations that are likely to be above the channel (called likely-on-channel), and locations that are not above the channel (called off-channel). A Mann-Whitney U test shows no significant difference ($p = 0.05$) in ablation between on-channel and off-channel locations. With regard to surface elevation changes, the Mann-Whitney U test shows that on-channel values are significantly different from off-channel ones ($p < 0.05$), whereas likely-on-channel values are not significantly different from off-channel values (Figure S12 and Table S5 in Supporting Information S1).

4. Discussion

Analysis of historical imagery has revealed a systematic increase in the frequency of surface collapse features due to "subglacial stoping" or "block caving" (Loewe, 1957; Paige, 1956) for a set of Swiss glaciers since 2000 (Figure 2), about 5–10 years after the onset of rapid climate warming for this region (Costa et al., 2018). This delay is not surprising as most Alpine glaciers show a lag in the onset of retreat with respect to temperature changes, primarily related to glacier surface slope (Jouvet et al., 2011; Zekollari et al., 2020). The collapse features (Figure S1 in Supporting Information S1) were found to occur predominantly in glaciers having margins comprised of thin ice (generally with a thickness of less than 50 m; Table S3 in Supporting Information S1) and with shallow surface slopes and bed slopes (both less than 23°; Table S7 in Supporting Information S1). Flow velocity calculations suggest these zones had almost no longitudinal ice flux (Figure S2c in Supporting Information S1) and reduced vertical channel closure rates (Figure S2b in Supporting Information S1). Given the importance of shallow surface slopes, glaciers currently showing collapse features are only likely to continue to do so if they do not retreat into zones of the steeper surface slope. The opposite might apply for glaciers not showing collapse if they retreat into a zone with a lower surface slope.

Intensive investigation of one of the 12 glaciers with collapse features showed that collapse was centered directly over a subglacial channel (Figure 3a). Remarkably, enhanced vertical deformation was observed above this channel for at least 600 m up the glacier (Figures 3b and 3c). Any void under a glacier should be subject to void-directed ice flow unless water pressure in the void equals the ice overburden pressure (Fountain & Walder, 1998; Nye, 1953). Enhanced vertical deformation above the subglacial channel indicates that the latter was not pressurized for some way up-glacier. The vertical deformation was not enough to close the void. Based on the analysis presented in Hooke (1984; Figure 2), with the thickness of ice at the snout of the glacier and a glacier bed slope that is marginally greater than the glacier surface slope, the channel is likely to be open. Our work importantly suggests that locally-increased vertical deformation rates on Alpine glaciers may be used to map the position of such subglacial channels flowing at atmospheric pressure.

The vertical deformation over the subglacial channel at the Glacier d'Otemma was approximately 0.2–0.3 m over a 16-day period (Figure 3c). Theoretical calculations using Hooke (1984) (Section S3.1 in Supporting Information S1) suggest a closure rate of 0.18 m per year if we assume a 5-m-diameter semi-circular channel. One explanation for a higher closure rate than predicted by theory is the deviation of the channel from a semi-circular shape, as observed in boreholes made at the Glacier d'Otemma during the summer of 2021, and reported for the Rhonegletscher by Church et al. (2021). An analysis using the theory for non-semi-circular conduits by Hooke et al. (1990) produces closure rate estimates over a 16-day period of ~0.03–0.13 m (Section S3.5 in Supporting Information S1), which is commensurate with our estimations.

Taking into account the DoD detection limit (±0.031 m), the 0.2–0.3 m of measured surface deformation is greater than theory. The question then becomes: Why are high vertical deformation rates maintained without returning the subglacial channel to a pressurized state? Field observations revealed large blocks of ice in the braid plain downstream from the glacier during the collapse event. We propose that as the ice overlying the subglacial channel close to the terminus is thin (~5–7 m; Figure S13 in Supporting Information S1) and as it creeps toward the channel, ice blocks fall off the ceiling (block caving; Paige, 1956). Thus, whilst there is an enhanced vertical deformation rate, basal ice is lost via subglacial caving rather than contributing to subglacial channel closure. These findings are supported by the results of a recent study of more than 1,400 esker enlargements that suggest ice-marginal subglacial channel collapse in the late stages of rapid ice sheet retreat (Dewald et al., 2021). This caving process is rarely considered a contributor to the mass balance of Alpine glaciers. We can get some idea of its comparable contribution; comparison of Figures 3a and 3b suggests vertical deformation that is about 20% of surrounding ablation for clear ice but similar in magnitude for zones of debris-covered ice. The snout marginal zone of the Glacier d'Otemma is about 500 m wide and 40% debris covered. Given that the vertical deformation occurs over a 10–20 m width, and assuming equilibrium between vertical deformation and subglacial channel evacuation of ice, it implies only a 2% increase in mass loss of ice. However, field evidence of large blocks, typically >1 m diameter, deposited in the proglacial margin during the collapse suggests that the collapse itself may be a much more significant contribution to snout margin retreat in years when it occurs. This merits investigation.

Two additional mechanisms may play a role in the development of collapse features that merit further investigation. The first relates to the greater sensitivity in the retreat of glaciers with collapse features to inter-annual summer temperature variation (Figure S11b in Supporting Information S1). This sensitivity may result from a reduced longitudinal flux in the snout margin of such glaciers, but also because of enhanced subglacial exposure to warm air during summers. The measured vertical deformation at the Glacier d'Otemma suggests a significant up-glacier extent of water flow at atmospheric pressure (Figures 3b and 3c) and hence subglacial exposure to warm air incursion. Temperature sensitivity may also result from the effects of warm tributary streams that enter the glacier at the snout margin.

The second mechanism to note is suggested in Figure 3a, which shows that the subglacial channel at the Glacier d'Otemma is meandering and that the collapse feature forms at a bend in the channel. The time-series images of collapse at the Glacier d'Otemma show that the collapse morphology has meander-parallel crevasses (Figure S15 in Supporting Information S1). The possibility that subglacial channels are sinuous has been recognized, notably in studies of dye breakout curves (Kohler, 1995) suggesting the presence of open-channel flow with walls comprised of ice and/or till that can be mechanically eroded. It is well-established that straight rivers that are able to erode their beds and/or banks tend to initiate meandering as a result of the inherent instability related to the effects of turbulent anisotropy on secondary circulation and which tends to grow as a function of time across a wide range of river scales (Dey & Ali, 2017). In theory, deviation from a glacier-longitudinal orientation exposes the channel to greater longitudinal fluxes and hence greater closure so meaning that subglacial channels cannot meander unless they can erode into bedrock. However, the low surface slopes and thin ice in the margins of the glaciers we found showing collapse (Figures S2a–S2e in Supporting Information S1), coupled with the possibility that the immediate margins of temperate glaciers may have zones of compression (Reinardy et al., 2019) would slow the rate of closure of laterally-oriented subglacial channels, especially if they are wide and flat. At the Otemma glacier with the estimated longitudinal velocities (1.29 m per year, Table S7 in Supporting Information S1) the more than 10-m-wide subglacial channel would only close by around 10%–15% per year. This would allow the maintenance of channels that meander. Thus, as glaciers thin and their longitudinal velocities fall, not only do subglacial channels close less readily, they may be increasingly able to maintain a meandering form, which in turn contributes to surface collapse. As technologies for mapping subglacial channels improve, it should become possible to test the hypothesis that meandering open channel flow under glacier snout margins with low longitudinal ice flux is a likely mechanism driving collapse.

5. Conclusions

The frequency of collapse features in Alpine glaciers has increased markedly since 2000. Such collapse is associated with glaciers that tend to have lower rates of longitudinal ice flux and so reduced compression and longitudinal closure. Low longitudinal flux is a consequence of glacier thinning related to a tendency for Alpine glaciers to have a negative mass balance due to climate warming. Glacier thinning leads to a long-term reduction of flux of accumulated ice into the ablation zone. Thus, the frequency of collapse at Alpine glacier margins is likely to increase as climate warming continues. The delay between the onset of warming (late 1980s) and the onset of increased collapse (year 2000) is not surprising given it may take some time for a long-term decrease in mass balance to translate into a reduction in snout marginal longitudinal ice flux. Not all retreating glaciers are likely to display collapse features at all times; given the dependence of collapse on low longitudinal ice flux, the snout margin should be in a zone of relatively low surface slope.

An intensive study of a collapse event for one glacier confirmed that collapse occurred over a subglacial channel flowing at atmospheric pressure. Two mechanisms are suggested to explain collapse formation: (a) up-glacier incursion of warm air and/or supply of warm water to the glacier snout margins and (b) development of subglacial channel meanders that can be maintained due to low longitudinal ice flux rates.

Data Availability Statement

The data supporting the conclusions meets FAIR principles and are supplied with this study under the following link: https://doi.org/10.5061/dryad.h18931zmh.

References

Arnold, N. (2005). Investigating the sensitivity of glacier mass-balance/elevation profiles to changing meteorological conditions: Model experiments for haut glacier D'Arolla, Valais, Switzerland. *Arctic Antarctic and Alpine Research*, *37*, 139–145. https://doi.org/10.1657/1523-0430(2005)037[0139:itsoge]2.0.co;2

Bartholomaus, T. C., Anderson, R. S., & Anderson, S. P. (2011). Growth and collapse of the distributed subglacial hydrologic system of Kennicott Glacier, Alaska, USA, and its effects on basal motion. *Journal of Glaciology*, *57*, 985–1002. https://doi.org/10.3189/002214311798843269

Church, G., Bauder, A., Grab, M., & Maurer, H. (2021). Ground-penetrating radar imaging reveals glacier's drainage network in 3D. *The Cryosphere*, *15*, 3975–3988. https://doi.org/10.5194/tc-15-3975-2021

Cuffey, K. M., & Paterson, W. S. B. (2010). *The physics of glaciers*. Academic Press.

Costa, A., Molnar, P., Stutenbecker, L., Bakker, M., Silva, T. A., Schlunegger, F., et al. (2018). Temperature signal in suspended sediment export from an Alpine catchment. *Hydrology and Earth System Sciences*, *22*(1), 509–528. https://doi.org/10.5194/hess-22-509-2018

Dewald, N., Lewington, E. L., Livingstone, S. J., Clark, C. D., & Storrar, R. D. (2021). Distribution, characteristics and formation of esker enlargements. *Geomorphology*, *392*, 107919. https://doi.org/10.1016/j.geomorph.2021.107919

Dey, S., & Ali, S. Z. (2017). Origin of the onset of meandering of a straight river. *Proceedings of the Royal Society A: Mathematical, Physical & Engineering Sciences*, *473*, 20170376. https://doi.org/10.1098/rspa.2017.0376

Diolaiuti, G. A., Maragno, D., D'Agata, C., Smiraglia, C., & Bocchiola, D. (2011). Glacier retreat and climate change: Documenting the last 50 years of Alpine glacier history from area and geometry changes of Dosde Piazzi glaciers (Lombardy Alps, Italy). *Progress in Physical Geography*, *35*, 161–182. https://doi.org/10.1177/0309133311399494

Egli, P., Irving, J., & Lane, S. (2021). Characterization of subglacial marginal channels using 3-D analysis of high-density ground-penetrating radar data. *Journal of Glaciology*, *67*, 759–772. https://doi.org/10.1017/jog.2021.26

Fischer, M., Huss, M., & Hoelzle, M. (2015). Surface elevation and mass changes of all Swiss glaciers 1980–2010. *The Cryosphere*, *9*, 525–540. https://doi.org/10.5194/tc-9-525-2015

Fountain, A. G., & Walder, J. S. (1998). Water flow through temperate glaciers. *Reviews of Geophysics*, *36*, 299–328. https://doi.org/10.1029/97rg03579

Gantayat, P., Kulkarni, A. V., & Srinivasan, J. (2014). Estimation of ice thickness using surface velocities and slope: Case study at Gangotri Glacier, India. *Journal of Glaciology*, *60*, 277–282. https://doi.org/10.3189/2014jog13j078

Gindraux, S., Boesch, R., & Farinotti, D. (2017). Accuracy assessment of digital surface models from unmanned aerial vehicles' imagery on glaciers. *Remote Sensing*, *9*, 186. https://doi.org/10.3390/rs9020186

GLAMOS. (1881–2020). *The Swiss glaciers 1880-2018/19, Glaciological Reports No 1-140, Yearbooks of the Cryospheric Commission of the Swiss Academy of Sciences (SCNAT)*. VAW/ETH Zurich. https://doi.org/10.18752/glrep_series

Grab, M., Mattea, E., Bauder, A., Huss, M., Rabenstein, L., Hodel, E., et al. (2021). Ice thickness distribution of all Swiss glaciers based on extended ground-penetrating radar data and glaciological modeling. *Journal of Glaciology*, 1–19. https://doi.org/10.1017/jog.2021.55

Haeberli, W., & Hölzle, M. (1995). Application of inventory data for estimating characteristics of and regional climate-change effects on mountain glaciers: A pilot study with the European Alps. *Annals of Glaciology*, *21*, 206–212. https://doi.org/10.1017/s0260305500015834

Haeberli, W., Hoelzle, M., Paul, F., & Zemp, M. (2007). Integrated monitoring of mountain glaciers as key indicators of global climate change: The European Alps. *Annals of Glaciology*, *46*, 150–160. https://doi.org/10.3189/172756407782871512

Hooke, R. L. (1984). On the role of mechanical energy in maintaining subglacial water conduits at atmospheric pressure. *Journal of Glaciology*, *30*, 180–187. https://doi.org/10.3189/s0022143000005918

Hooke, R. L., Laumann, T., & Kohler, J. (1990). Subglacial water pressures and the shape of subglacial conduits. *Journal of Glaciology*, *36*, 67–71. https://doi.org/10.3189/s0022143000005566

James, M. R., Antoniazza, G., Robson, S., & Lane, S. N. (2020). Mitigating systematic error in topographic models for geomorphic change detection: Accuracy, precision and considerations beyond off-nadir imagery. *Earth Surface Processes and Landforms*, *45*, 2251–2271. https://doi.org/10.1002/esp.4878

Jarque, C. M., & Bera, A. K. (1980). Efficient tests for normality, homoscedasticity and serial independence of regression residuals. *Economics Letters*, *6*, 255–259. https://doi.org/10.1016/0165-1765(80)90024-5

Jouvet, G., Huss, M., Funk, M., & Blatter, H. (2011). Modelling the retreat of Grosser Aletschgletscher, Switzerland, in a changing climate. *Journal of Glaciology*, *57*, 1033–1045. https://doi.org/10.3189/002214311798843359

Kellerer-Pirklbauer, A., & Kulmer, B. (2019). The evolution of brittle and ductile structures at the surface of a partly debris-covered, rapidly thinning and slowly moving glacier in 1998–2012 (Pasterze Glacier, Austria). *Earth Surface Processes and Landforms*, *44*, 1034–1049. https://doi.org/10.1002/esp.4552

Kohler, J. (1995). Determining the extent of pressurized flow beneath Storglaciären, Sweden, using results of tracer experiments and measurements of input and output discharge. *Journal of Glaciology*, *41*, 217–231. https://doi.org/10.1017/s0022143000016129

Konrad, S. K. (1998). Possible outburst floods from debris-covered glaciers in the Sierra Nevada, California. *Geografiska Annaler—Series A: Physical Geography*, *80*, 183–192. https://doi.org/10.1111/j.0435-3676.1998.00036.x

Lane, S. N., Westaway, R. M., & Murray Hicks, D. (2003). Estimation of erosion and deposition volumes in a large, gravel-bed, braided river using synoptic remote sensing. *Earth Surface Processes and Landforms: The Journal of the British Geomorphological Research Group*, *28*, 249–271. https://doi.org/10.1002/esp.483

Lindström, E. (1993). Esker enlargements in Northern Sweden. *Geografiska Annaler - Series A: Physical Geography*, *75*, 95–110. https://doi.org/10.2307/521028

Loewe, F. (1957). Subglacial stoping or block caving. *Journal of Glaciology*, *3*, 152–152. https://doi.org/10.3189/s0022143000024552

Mann, H. B., & Whitney, D. R. (1947). On a test of whether one of two Random variables is stochastically larger than the other. The *Annals of Mathematical Statistics*, *18*, 50–60. https://doi.org/10.1214/aoms/1177730491

Messerli, A., & Grinsted, A. (2015). Image georectification and feature tracking toolbox: ImGRAFT. *Geoscientific Instrumentation, Methods and Data Systems*, *4*, 23–34. https://doi.org/10.5194/gi-4-23-2015

Millan, R., Mouginot, J., Rabatel, A., Jeong, S., Cusicanqui, D., Derkacheva, A., & Chekki, M. (2019). Mapping surface flow velocity of glaciers at regional scale using a multiple sensors approach. *Remote Sensing*, *11*, 2498. https://doi.org/10.3390/rs11212498

Nye, J. F. (1953). The flow law of ice from measurements in glacier tunnels, laboratory experiments and the Jungfraufirn borehole experiment. *Proceedings of the Royal Society of London - Series A: Mathematical and Physical Sciences*, *219*, 477–489. https://doi.org/10.1098/rspa.1953.0161

Oerlemans, J., & Knap, W. H. (1998). A 1 year record of global radiation and albedo in the ablation zone of Morteratschgletscher, Switzerland. *Journal of Glaciology*, *44*, 231–238. https://doi.org/10.1017/s0022143000002574

Paige, R. (1956). Subglacial stoping or block caving: A type of glacier ablation. *Journal of Glaciology*, *2*, 727–729. https://doi.org/10.3189/s0022143000024977

Paul, F., Kääb, A., Maisch, M., Kellenberger, T., & Haeberli, W. (2004). Rapid disintegration of Alpine glaciers observed with satellite data. *Geophysical Research Letters*, *31*, 2004GL020816. https://doi.org/10.1029/2004gl020816

Reinardy, B. T. I., Booth, A. D., Hughes, A. L. C., Boston, C. M., Åkesson, H., Bakke, J., et al. (2019). Pervasive cold ice within a temperate glacier—Implications for glacier thermal regimes, sediment transport and foreland geomorphology. *The Cryosphere*, *13*, 827–843. https://doi.org/10.5194/tc-13-827-2019

Rippin, D. M., Pomfret, A., & King, N. (2015). High resolution mapping of supra-glacial drainage pathways reveals link between micro-channel drainage density, surface roughness and surface reflectance. *Earth Surface Processes and Landforms*, *40*, 1279–1290. https://doi.org/10.1002/esp.3719

Rossini, M., Di Mauro, B., Garzonio, R., Baccolo, G., Cavallini, G., Mattavelli, M., et al. (2018). Rapid melting dynamics of an alpine glacier with repeated UAV photogrammetry. *Geomorphology*, *304*, 159–172. https://doi.org/10.1016/j.geomorph.2017.12.039

Shreve, R. L. (1972). Movement of water in glaciers. *Journal of Glaciology*, *11*, 205–214. https://doi.org/10.3189/s002214300002219x

Sommer, C., Malz, P., Seehaus, T. C., Lippl, S., Zemp, M., & Braun, M. H. (2020). Rapid glacier retreat and downwasting throughout the European Alps in the early 21 st century. *Nature Communications*, *11*, 1–10. https://doi.org/10.1038/s41467-020-16818-0

Stocker-Waldhuber, M., Fischer, A., Keller, L., Morche, D., & Kuhn, M. (2017). Funnel-shaped surface depressions—Indicator or accelerant of rapid glacier disintegration? A case study in the Tyrolean Alps. *Geomorphology*, *287*, 58–72. https://doi.org/10.1016/j.geomorph.2016.11.006

SwissTopo. (2021). Retrieved from https://map.geo.admin.ch

Vincent, C., Kappenberger, G., Valla, F., Bauder, A., Funk, M., & Le Meur, E. (2004). Ice ablation as evidence of climate change in the Alps over the 20th century. *Journal of Geophysical Research*, *109*, 2003JD003857. https://doi.org/10.1029/2003jd003857

Westoby, M. J., Brasington, J., Glasser, N. F., Hambrey, M. J., & Reynolds, J. M. (2012). `Structure-from-motion' photogrammetry: A low-cost, effective tool for geoscience applications. *Geomorphology*, *179*, 300–314. https://doi.org/10.1016/j.geomorph.2012.08.021

Zekollari, H., Huss, M., & Farinotti, D. (2019). Modelling the future evolution of glaciers in the European Alps under the EURO-CORDEX RCM ensemble. *The Cryosphere*, *13*, 1125–1146. https://doi.org/10.5194/tc-13-1125-2019

Zekollari, H., Huss, M., & Farinotti, D. (2020). On the imbalance and response time of glaciers in the European Alps. *Geophysical Research Letters*, *47*, 2019GL085578. https://doi.org/10.1029/2019gl085578

References From the Supporting Information

Glen, J. W. (1958). The flow law of ice: A discussion of the assumptions made in glacier theory, their experimental foundations and consequences. *IASH Publication*, *47*, e183.

James, M. R., Chandler, J. H., Eltner, A., Fraser, C., Miller, P. E., Mills, J. P., et al. (2019). Guidelines on the use of structure-from-motion photogrammetry in geomorphic research. *Earth Surface Processes and Landforms*, *44*, 2081–2084. https://doi.org/10.1002/esp.4637

James, M. R., Robson, S., & Smith, M. W. (2017). 3-D uncertainty-based topographic change detection with structure-from-motion photogrammetry: Precision maps for ground control and directly georeferenced surveys. *Earth Surface Processes and Landforms*, *42*, 1769–1788. https://doi.org/10.1002/esp.4125

Nienow, P., Sharp, M., & Willis, I. (1998). Seasonal changes in the morphology of the subglacial drainage system, Haut Glacier d'Arolla, Switzerland. *Earth Surface Processes and Landforms*, *23*, 825–843. https://doi.org/10.1002/(sici)1096-9837(199809)23:9<825::aid-esp893>3.0.co;2-2

Paul, F., Azzoni, R. S., Fugazza, D., Le Bris, R., Nemec, J., Paul, F., et al. (2019). *GLIMS glacier database*. National Snow and Ice Data Center. https://doi.org/10.7265/N5V98602